Journal of Nuclear Medicine, published on July 25, 2024 as doi:10.2967/jnumed.124.267482

# Development of a $^{213}$Bi-Labeled Pyridyl Benzofuran for Targeted α-Therapy of Amyloid-β Aggregates

Aidan A. Bender[1], Emily K. Kirkeby[2], Donna J. Cross[3], Satoshi Minoshima[3], Andrew G. Roberts[2], and Tara E. Mastren[1]

[1]*Nuclear Engineering Program, University of Utah, Salt Lake City, Utah;* [2]*Department of Chemistry, University of Utah, Salt Lake City, Utah; and* [3]*Department of Radiology, University of Utah, School of Medicine, Salt Lake City, Utah*

Alzheimer disease is a neurodegenerative disorder with limited treatment options. It is characterized by the presence of several biomarkers, including amyloid-β aggregates, which lead to oxidative stress and neuronal decay. Targeted α-therapy (TAT) has been shown to be efficacious against metastatic cancer. TAT takes advantage of tumor-localized α-particle emission to break disease-associated covalent bonds while minimizing radiation dose to healthy tissues due to the short, micrometer-level, distances traveled. We hypothesized that TAT could be used to break covalent bonds within amyloid-β aggregates and facilitate natural plaque clearance mechanisms. **Methods:** We synthesized a $^{213}$Bi-chelate–linked benzofuran pyridyl derivative (BiBPy) and generated [$^{213}$Bi]BiBPy, with a specific activity of 120.6 GBq/μg, dissociation constant of 11 ± 1.5 nM, and logP of 0.14 ± 0.03. **Results:** As the first step toward the validation of [$^{213}$Bi]BiBPy as a TAT agent for the reduction of Alzheimer disease–associated amyloid-β, we showed that brain homogenates from APP/PS1 double-transgenic male mice (6–9 mo old) incubated with [$^{213}$Bi]BiBPy exhibited a marked reduction in amyloid-β plaque concentration as measured using both enzyme-linked immunosorbent and Western blotting assays, with a half-maximal effective concentration of 3.72 kBq/pg. **Conclusion:** This [$^{213}$Bi]BiBPy-concentration–dependent activity shows that TAT can reduce amyloid plaque concentration in vitro and supports the development of targeting systems for in vivo validations.

**Key Words:** targeted α-therapy; Alzheimer disease; radiochemistry; amyloid-β; pyridyl benzofuran

**J Nucl Med 2024; 00:1–6**
DOI: 10.2967/jnumed.124.267482

Alzheimer disease (AD) is one of the leading causes of dementia and the sixth leading cause of death in the United States (*1*). By 2050, the number of people diagnosed with AD is expected to more than double (*1*). The economic burden of AD reaches beyond easily calculable health care services (>$200 billion annually), to the burden of unpaid caregivers. Currently, there are limited treatment options for AD, with most Food and Drug Administration–approved regimens being palliative rather than curative. Recently, lecanemab was Food and Drug Administration–approved as an antibody-based treatment for the reduction of amyloid-β plaques (*2*). This treatment shows a stronger connection between treating amyloid-β and slowing cognitive decline than do previous treatments (*3*). The development of therapies to treat AD, and other neurodegenerative diseases, defines a rapidly growing research area (*4*).

However, there is some debate regarding the best biochemical target for AD (*5*). Although the amyloid hypothesis is the most researched route for treatment of AD (*6*), there remains some doubt as to the efficacy of such treatments. Other targets, such as tau protein fibrils, have also come to light as potential therapy routes (*7*). The multifactorial origin of AD makes it difficult to select a pharmaceutical target. Since more traditional modalities have struggled to treat AD, research has broadened to include methods beyond the biochemical.

An area of research with promise is the use of whole-brain, low-dose ionizing radiation (LDIR) (*8*). This therapy makes use of x-ray machines to deliver ionizing radiation to the brain and has been shown to activate immune responses (*9,10*). Either through the activation of the immune system or through a more direct mechanism, LDIR therapy has demonstrated the ability to reduce key biomarker concentrations (*11*). LDIR treatments in mice resulted in improved cognitive function (*12*), and stage 1 trials in human patients showed a positive effect on emotional and cognitive expressions of AD (*13–15*). LDIR is not the only nonpharmacologic method being explored for AD, as it is complemented by research in ultrasonication (*16*) and electric field therapy (*17*). Although LDIR shows promise, it also comes with other concerns, such as the widespread radiation dose. There are, however, other ionizing radiation therapies that can minimize healthy-tissue doses.

Targeted α-therapy (TAT) is an area of growing development (*18*). Within this paradigm, α-particle (a helium ion)–emitting radionuclides are selectively delivered to a target via their linkage to a small molecule or biologic vector. When an α-particle–emitting radionuclide decays, it releases 4–10 MeV of kinetic energy (*19*), which is deposited into the surroundings through electrostatic interactions (*20*). Because of the charged nature of α-particles, as well as their small size, these interactions occur within only a few micrometers of the location of radioactive decay (*21*). α-particles, therefore, travel only 1–10 cell lengths in tissue, generating a controlled and localized dose. This is measured as a linear energy transfer. TAT is focused primarily on developing cancer treatments, with the high linear energy transfer of α-particles being used to break double-stranded DNA in cancer cells, resulting in cell death and generating radical oxygen species that further damage the cancer cells (*21,22*). TAT has been shown to be potent in metastatic cancers (*23*), for which other radiotherapies may be less efficacious because of lower linear energy transfer resulting in significant doses to healthy tissues (*21,24*).

Although TAT is established for the treatment of cancers, the use of physical energy transfer to break covalent bonds may be advantageous in other diseases. We hypothesize that TAT will break covalent bonds within AD-associated amyloid-β aggregates

Received Jan. 23, 2024; revision accepted Jun. 25, 2024.
For correspondence or reprints, contact Tara E. Mastren (tara.mastren@utah.edu).
Published online Jul. 25, 2024.

to facilitate natural plaque clearance mechanisms. In addition to the breaking apart of plaques by energetic particles, we hypothesize that a localized immune response would be generated by TAT, like the more generalized immune response to LDIR (*25*). Because of the high linear energy transfer of α-particles, the regions of tissue that would activate an immune response would be much smaller than in LDIR. Localization of the immune response, we hypothesize, may also avoid overactivation of the immune response leading to inflammation.

The development of methodologies for the treatment of AD relies on appropriate targeting platforms. In the past, several platforms have been designed as amyloid-β–selective targeting vectors that cross the blood–brain barrier (BBB) (*26*). The BBB has been one of the major challenges in developing therapeutic systems for AD, as foreign molecules can be barred from entry, and larger biomolecules, such as antibodies, enter slowly (*27*). For this reason, small molecules that mimic thioflavin-T (**1,** Fig. 1) were developed to enable a range of AD-specific biomarker imaging modalities. Selected PET and SPECT imaging agents include [$^{11}$C]PIB (**2,** Fig. 1), [$^{18}$F]flutemetamol (**3,** Fig. 1), [$^{123}$I]IMPY (**4,** Fig. 1), and [$^{99m}$Tc]BAT-Bp-2 (**5,** Fig. 1) (*28*). Notably, **3** is a Food and Drug Administration–approved PET imaging agent using $^{18}$F (half-life, 109.7 min) (*29*). Borrowing a synthetic route developed for **3,** we previously synthesized an $^{211}$At-labeled derivative (**6,** Fig. 1) (half-life, 7.2 h) as a potential TAT therapeutic for AD (*30*). Although $^{211}$At is advantageous because of its ready incorporation from boronic acid precursors (**7** [Fig. 1] → **6**) (*31*) and single–α-emitting decay chains, its short half-life and limited availability (*32–34*) made assessment of the therapeutic properties of **6** challenging. To address these issues, we proposed the synthesis and evaluation of a $^{213}$Bi-containing agent ([$^{213}$Bi]BiBPy [**8**], Fig. 2A). Like $^{211}$At, $^{213}$Bi has a short half-life (46 min) and decays with the emission of a single α-particle (Fig. 2B), but importantly, $^{213}$Bi is accessible in-house from its parent radionuclide, $^{225}$Ac (half-life, 9.92 d), through the creation of an $^{225}$Ac/$^{213}$Bi radionuclide generator system. Since $^{213}$Bi cannot be directly bound to the targeting vector, we designed a $^{213}$Bi-chelate–linked benzofuran pyridyl derivative (**8**), drawing inspiration from **5** (*28*). We proposed that **8** could derive from the assembly of known precursors **9, 10,** and **11** (Fig. 2). Although other chelates could be readily linked to **10,** we selected cyclohexane (CHX)-A″-diethylenetriaminepentaacetic acid (DTPA) because of its favorable binding kinetics to $^{213}$Bi (*35*). Here, we report the synthesis, radiolabeling, and in vitro evaluation of **8,** which we hypothesized would reduce plaque burden after TAT treatment of AD.

## MATERIALS AND METHODS

The full materials and methods are provided in the supplemental materials (available at http://jnm.snmjournals.org).

### Radiolabeling to Prepare 8

To radiolabel **17** (supplemental materials) and afford **8,** 0.37 MBq of $^{213}$Bi was incubated with **17** in 0.1 M ammonium acetate (pH 5.5) for 10 min at 37°C. This sample (**8**) was then analyzed by high-performance liquid chromatography (HPLC), by which the retention time of [$^{Nat}$Bi]BiBPy was tracked by ultraviolet–visible spectroscopy,

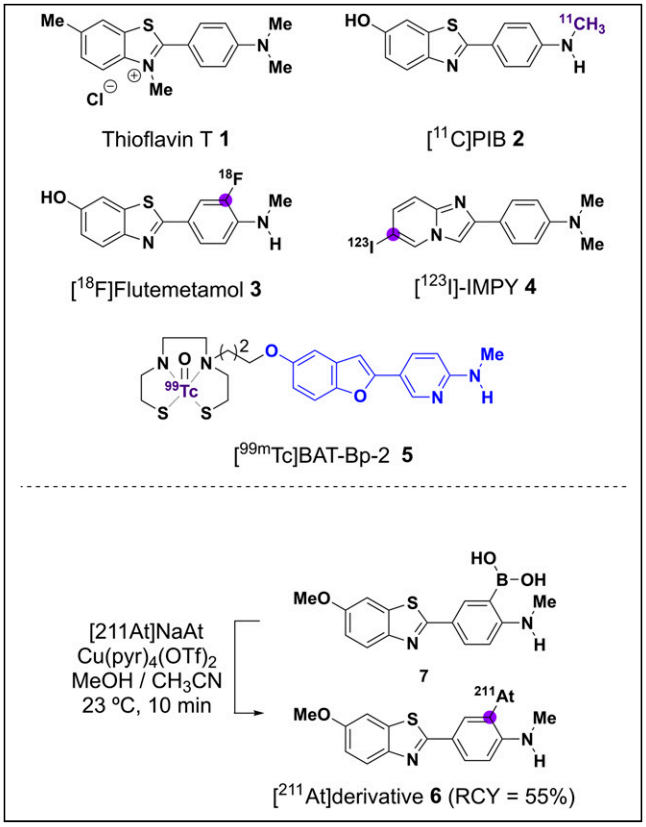


**FIGURE 1.** Previously reported amyloid imaging agents and derivative labeled with $^{211}$At, as method of TAT for AD. RCY = radiochemical yield.

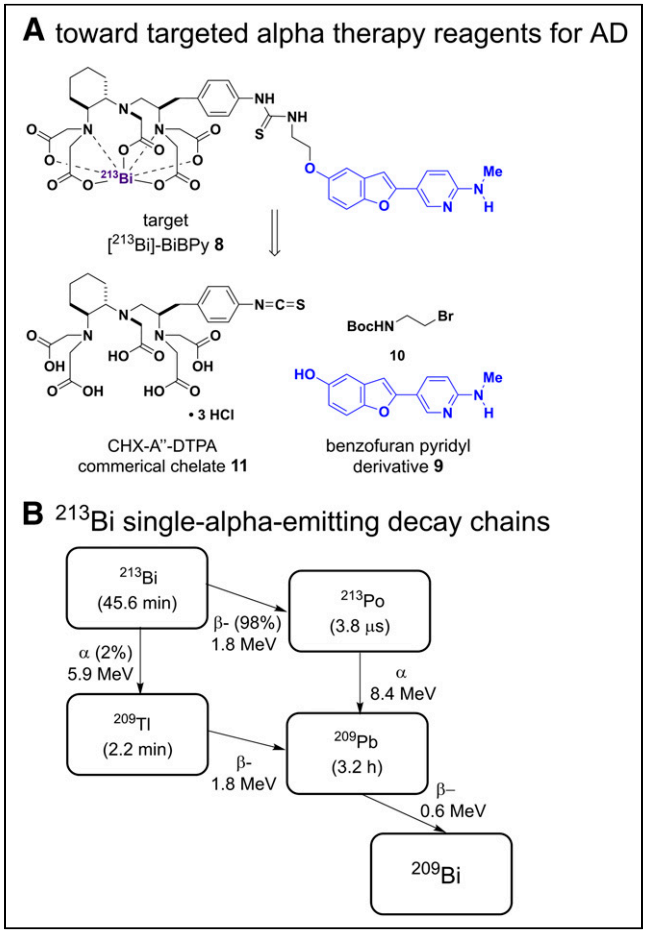


**FIGURE 2.** (A) Retrosynthetic analysis of TAT reagent for AD. (B) $^{213}$Bi decay chain.

and the retention time of **8** was tracked by collecting fractions and counting them on a γ-counter. Furthermore, specific activity was calculated by serial dilution of **8** with a constant 0.296 MBq of $^{213}$Bi and analysis of the bound $^{213}$Bi fraction by radio-HPLC.

### Partition Coefficient and Stability Constant

The partition coefficient was measured by preparing a tracer of 0.011 μmol of **17** mixed with 0.0525 MBq of $^{213}$Bi and 0.1 mM $^{nat}BiCl_3$ to fully complex **17.** Solutions of 1-octanol and phosphate-buffered saline (pH 7.4) were presaturated with one another. The presaturated solutions were spiked with 15 μL of the tracer solution and vortexed for 30 min. Aliquots of each phase were taken and measured with a γ-counter, as well as injected on analytic HPLC after dilution in HPLC buffers.

Amyloid-β peptides were aggregated by reconstituting amyloid-β (1–42) peptide (Thermo Scientific). Samples were prepared by combining 100 μL of the amyloid-β peptide solution (final concentration, 0.204 μM), the BiBPy tracer (final concentration, 8.31 nM), and one of the **1** dilution series (final concentration, 0.456–4.56E−10 M). These solutions were incubated at 37°C for 1 h and then filtered. The filtered solutions were counted on a γ-counter to determine the fraction of BiBPy bound to the aggregates.

### Brain Homogenate Incubation and Ex Vivo Imaging

All animal experiments were approved by the University of Utah's Institutional Animal Care and Use Committee in compliance with all federal mandates for animal testing.

To determine the response of amyloid-β plaques in brain homogenate to α-decay in vitro, aliquots of brain homogenate solutions were incubated with free $^{213}$Bi, **8,** and a negative control solution. After 24 h, the concentration of amyloid-β plaques was measured by enzyme-linked immunosorbent assay and Western blot.

Compound **15** (Fig. 3) was used to prepare fluorescein-functionalized **12** (Fig. 3), in which the chelate is replaced by fluorescein. Tissue sections of AD mice and wild-type control mice were incubated with 0.1% propidium iodide before being incubated with either 0.1% thioflavin-S or **12.** The slides were imaged using an Axio Scan.Z1 slide scanner (Ziess).

## RESULTS

### Synthesis of 8 and Fluorescent BPy 12

Toward target **8** and fluorescent probe **12,** we synthesized precursor **9** (Fig. 3). Following reported conditions (*28*), we coupled boronic acid (**13,** Fig. 3) with 5-bromopyridyl (**14,** Fig. 3) and demethylated (**S-1,** supplemental materials) on treatment with boron tribromide to obtain **9** in 69.7% yield over 2 steps (Fig. 3A). Next, **9** was alkylated with *tert*-butyl(2-bromoethyl)carbamate (**10**), and **S-2** (supplemental materials) was deprotected using acidic conditions to furnish ammonium-**14** (64%, over 2 steps). Taking advantage of isothiocyanate reactivity, ammonium-**14** linked the fluorescent tag (fluorescein isothiocyanate [**16**]) and bichelate (*p*-SCN-Bn-CHX-A″-DTPA [**11**]). On reaction of **15** with **16** under basic conditions, fluorescein derivative **12** was obtained in 39% yield after purification by preparative HPLC (Fig. 3B). On reaction of **15** with **11** under basic conditions, the bichelate precursor, BPy (**S-3,** supplemental materials), was obtained in 43% yield after purification by preparative HPLC (Fig. 3C). Full synthesis and analysis details are presented in Supplemental Figures 1–11.

### $^{225}$Ac/$^{213}$Bi Generator and Radiolabeling to Prepare 8

The $^{225}$Ac/$^{213}$Bi generator was eluted daily during operation. $^{213}$Bi eluted off the column with an average radiochemical yield of 78% ± 4.9% in 1 mL of 0.1 M HCl/0.1 M NaI. The average

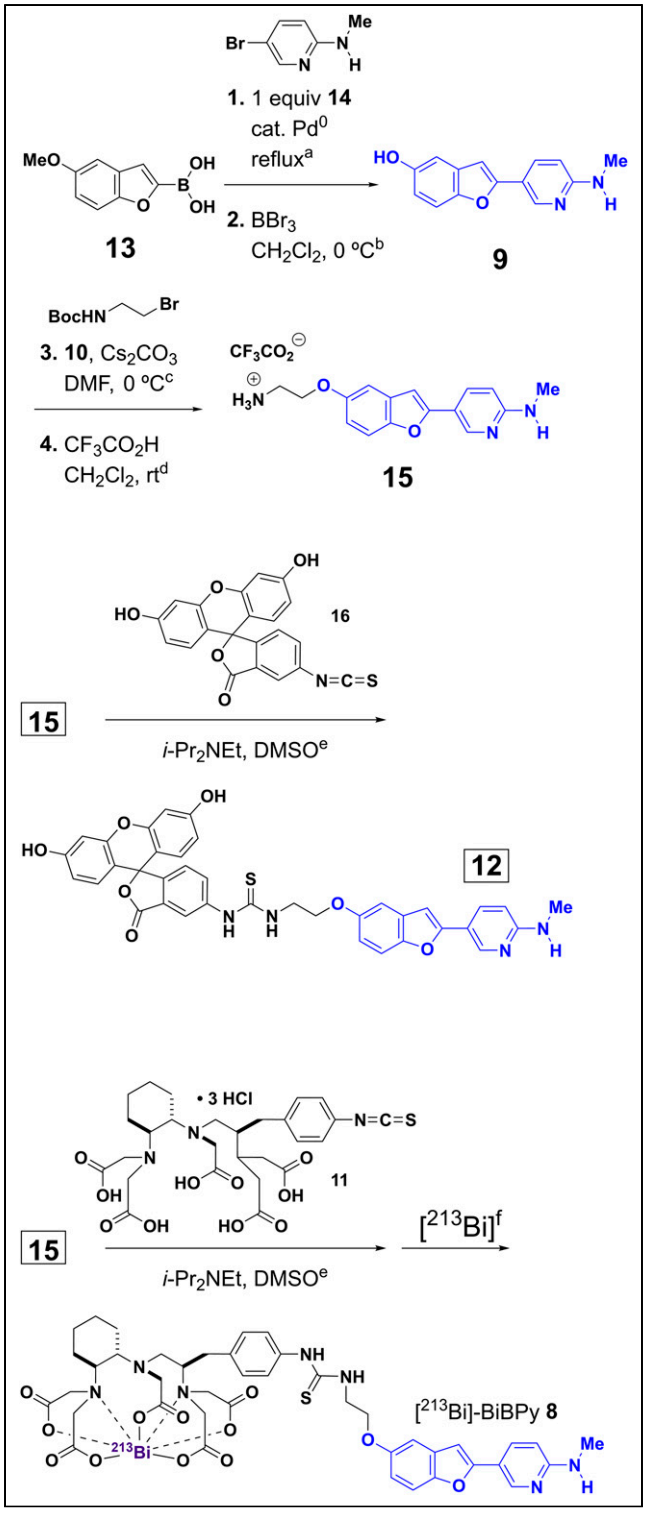


**FIGURE 3.** Synthesis of fluorescent BPy and **8.**

breakthrough of $^{225}$Ac was 0.03% ± 0.01%. Accordingly, BPy (**S-3**) was radiolabeled with $^{213}$Bi, obtaining **8** in an average radiochemical yield of 97% ± 1.5%. HPLC analyses of **8** ($^{213}$Bi counts, red) and [$^{209}$Bi]BiBPy (**S-4**, supplemental materials) (ultraviolet–visible spectroscopy λ = 330 nm, black) showed retention times of about 11.3 min, supporting the identity of the radiolabeled conjugate (Fig. 4A). The specific activity of **8** was

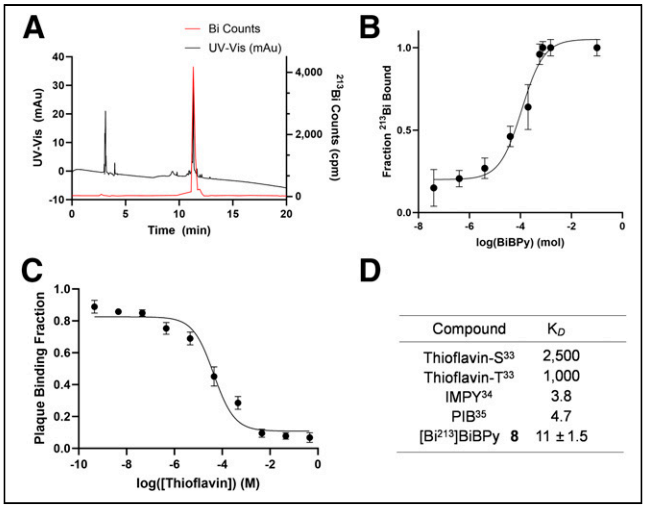


**FIGURE 4.** (A) Ultraviolet–visible spectroscopy (UV-Vis) and $^{213}$Bi counts of BiBPy. (B) Specific activity of **8**: 120.6 GBq/μg BiBPy. (C) Binding competition assay against thioflavin-S; **8** dissociation constant ($K_D$) is 11 ± 1.5 nM. (D) Comparison of **8** $K_D$ to other small-molecule agents for amyloid plaques.

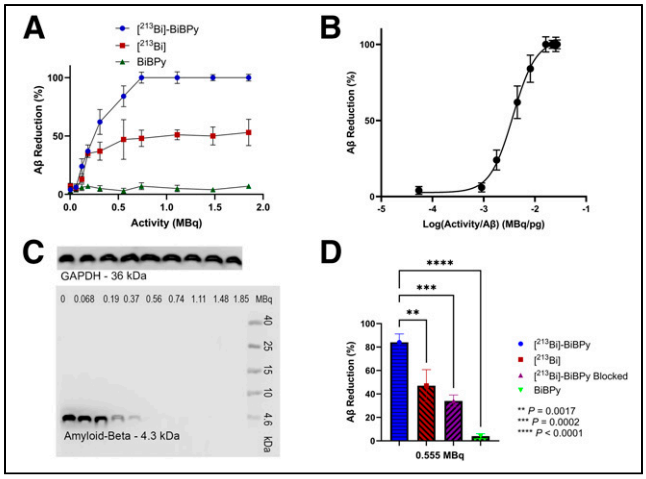


**FIGURE 5.** (A) Amyloid-β (Aβ) plaque reduction, measured by enzyme-linked immunosorbent assay, as function of increasing $^{213}$Bi activity, free or targeted. (B) Fitting of amyloid-β reduction as function of activity. (C) Western blot analysis of amyloid-β after exposure to [$^{213}$Bi]BiBPy confirms enzyme-linked immunosorbent assay trend of reduced plaque concentration. (D) When targeting of **8** is not blocked, plaque concentration is markedly less than when targeting is blocked (here, by **1**). GAPDH = glyceraldehyde 3-phosphate dehydrogenase.

measured to be 120.6 GBq/μg, or 69.2% of the theoretic maximum (Fig. 4B).

### Lipophilicity

LogP, a measure of lipophilicity, is one tool used to determine transport across the BBB. For passive transport, logP is 0.1–3.5 (*28*). We measured the logP of **8** to assess its likelihood of crossing the BBB. The logP was 0.14 ± 0.03. This value is lower than the logP of other compounds with smaller, less charged chelates (*28*). Although 0.14 is within the ideal range, the uncertainty of this measurement suggests that passive diffusion may negatively affect the rate at which this complex crosses the BBB.

### Binding Affinity

The binding affinity of **8** was measured by performing an inhibition assay against **1** (Fig. 4C). The inhibition constant of **8** was measured using the Cheng–Prusoff equation (Fig. 4D). Compared with other standards, such as **2** and **4, 8** has a slightly larger inhibition constant (*36,37*). The dissociation constant of 11 ± 1.5 for **8** is consistent with that reported for benzofuran pyridyl derivatives without a chelate group (*28*), suggesting that the addition of the CHX-A″-DTPA chelate does not reduce the binding constant.

### In Vitro Analysis

The ability of TAT to reduce amyloid-β concentration was demonstrated in vitro. When **8** was incubated with brain homogenate, a dose-dependent reduction in amyloid-β was observed (Fig. 4). This reduction was measured using both enzyme-linked immunosorbent assays (Figs. 5A and 5B) and Western blot assays (Fig. 5C). Some reduction of amyloid-β was observed when incubating with free $^{213}$Bi, but at significantly lower levels ($P < 0.0001$). We hypothesize that this reduction is caused by amyloid-β plaques scavenging metal ions in solution (*38*). In an experiment in which amyloid-β was incubated first with **1** (blocking binding sites) followed by treatment with **8,** the result was a minimized reduction of amyloid-β ($P = 0.0002$) (Fig. 5D). This result further suggests the specificity of **8.** The dose response was determined by fitting the logarithmic activity used per mass of amyloid-β present in the samples (Fig. 5B). A value of 0.01488 ± 0.0006 MBq/pg of amyloid-β was measured to be the dose needed for 50% reduction of amyloid-β in vitro.

### Ex Vivo Analysis

APP/PS1 double-transgenic and wild-type control mice were euthanized and the brains removed and used to generate 10-μm-thick sections. Representative sections were stained to corroborate the ex vivo binding of **8,** using **12** (Fig. 6). Thioflavin-S staining was used

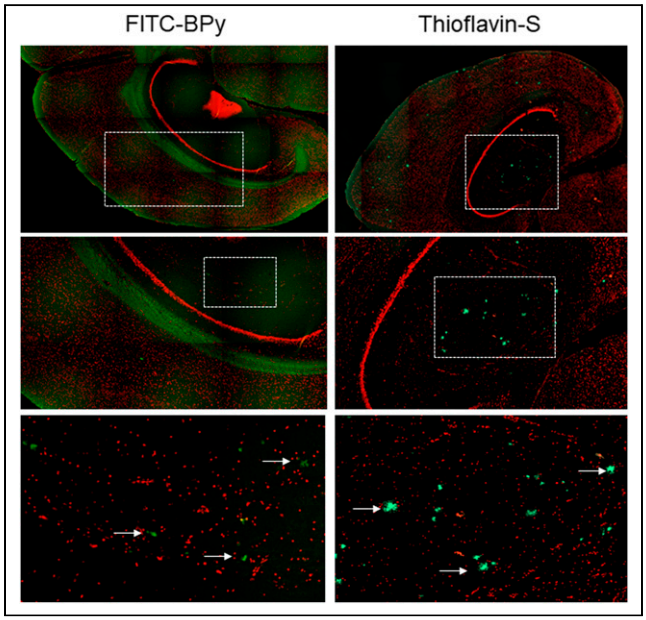


**FIGURE 6.** **12**-stained and thioflavin-S–stained tissue sections from representative APP/PS1 double-transgenic mice display presence of plaques (fluoresces green; white arrows). Propidium iodide (fluoresces red) is used as counterstain.

as a positive control (Fig. 6), and wild-type mice were used as a negative control (*39*). Propidium iodide was used throughout as a counterstain. Thioflavin-S staining shows a consistent, dense presence of plaques, particularly in the cortex, with minimal off-site binding of the stain. Compound **12** also suggests the presence of plaques in the cortex but stains them less intensely, with more off-site binding. It is known that benzofuran and benzothiazole derivatives can bind white matter in an off-target manner (*40*), suggesting that continued investigation of a targeting vector to lower white matter binding is vital.

## DISCUSSION

There are limited therapeutic routes for AD treatment. Most target the symptoms of AD rather than the underlying causes of the disease (*4,41*). LDIR, which has shown promise in treating symptoms in recent years, has also been suggested as a therapeutic for the underlying biomarkers, as studies have suggested plaque reduction and improved symptoms in animal models and human trials (*8–15*). With LDIR studies as inspiration, our hypothesis applies TAT toward the same target. In vitro, this hypothesis is supported by stark plaque reduction in the presence of **8.** TAT has the advantage of requiring a lower dose of radiation, as well as using targeting vectors to minimize the healthy-tissue dose. Although these initial in vitro studies cannot fully assess off-target doses, further in vivo studies are hypothesized to reinforce these results.

The high radiochemical purity and specific activity of compounds such as **8** are critical for pursuing further optimizations and in vivo studies. One of the major hurdles for AD therapy research is the BBB, which must be overcome. Although the charged nature of CHX-A″-DTPA complexing with $^{213}$Bi is expected to change the lipophilicity of the targeting molecule, the measured logP may suggest that crossing of the BBB is still possible and should be confirmed with in vivo biodistribution studies. In addition to passive crossing of the BBB, other methods of allowing transportation into the brain could be explored, such as ultrasound disruption (*42*). These molecules can cross the BBB more quickly than antibodies, providing a platform for radionuclides with short half-lives. In addition to these options for crossing the BBB, the successful reduction of plaques in vitro also suggests that previous $^{211}$At-labeled flutemetamol derivatives (**3**) should be developed and evaluated in vivo (*30*). Halogenated derivatives (e.g., fluorine, iodine, and astatine) of the flutemetamol scaffold provide an alternative to the chelate-incorporation strategy and may be more suitable to cross the BBB.

The brain homogenate studies show a strong response of plaques to TAT. Although the scavenging of metal ions in solution also showed a response, the significantly ($P < 0.0001$) higher response to the targeted radionuclides demonstrates the efficacy of the targeted approach. At the same time, other proteins in the homogenate solution did not appear to be affected, as the Western blot studies showed that the GAPDH control bands did not differ across increasing dose. This indicates a lack of off-target damage but cannot fully assess healthy-tissue dose. Reduction of plaques below the detection limits of both enzyme-linked immunosorbent assay (<10 pg/mL) and Western blot (<100 pg) strongly supports the hypothesis that TAT can reduce plaque burden. To further support this hypothesis, studies should be done in vivo.

On the basis of the initial success of in vitro reduction of amyloid plaques with TAT, further characterization of the targeting system should be performed. The in vivo biodistribution of **8** should be characterized. APP/PS1 double-transgenic mice will be used to establish this biodistribution, as well as to perform autoradiography to confirm the initial binding studies suggested by ex vivo analysis with **12.** These studies will be used to calculate toxicity as well as dose estimates for plaques and observation of plaque reduction in vivo. With initial studies suggesting that off-target binding is possible with this benzofuran derivative, other targeting vectors are also worth considering, whether it be another small molecule or a peptide. Since the library of amyloid-targeting vectors is moderately sized and growing, another system may prove ideal. Once a targeting vector is optimized and its biodistribution established, in vivo plaque response to TAT can be measured to further explore the hypothesis presented in this work. Furthermore, the biologic response to TAT must be considered. Since the immune system is activated in LDIR, the hypothesis is that localized responses would be generated at the site of dose deposition. Therefore, the immune system should be studied to elicit the type of response and its effect on the therapy. We plan to study localized microglia activity as well as inflammatory cytokines to assess this.

When in vivo studies are being planned, attention will be given to the age and disease state of subjects in addition to the sex. It has been shown that early and later disease states have a different response to LDIR, namely that earlier treatment resulted in reduction of plaques and inflammation markers whereas later treatments had only a cognitive impact (*43–45*). Identifying the stage of the disease at which treatment is most beneficial is an important marker for the future of this work. Furthermore, it has been shown that female mice and rats respond differently from their male counterparts, with no reduction in amyloid-β and minimal inflammatory responses (*46*). Differences in sex have been seen in other treatment modalities as well and are an important factor that must be considered when designing protocols.

## CONCLUSION

We prepared and evaluated a $^{213}$Bi-labeled benzofuran pyridyl derivative, **8,** and an orthogonal fluorescent derivative, **12,** to demonstrate the potential of a TAT strategy for the treatment of amyloid-β aggregate–associated diseases. Initial experiments show that **8** exhibits binding affinity like that previously reported for amyloid-β aggregate–selective compounds and demonstrates utility as a TAT agent by reducing the concentration of amyloid-β aggregates in vitro and in a dose-dependent manner. These studies show that physical energy, via TAT, can significantly reduce amyloid-β aggregates, supporting the further development of TAT approaches to clear amyloid-β aggregates associated with AD and other neurodegenerative diseases.

## DISCLOSURE

This research was supported by the University of Utah Departments of Chemistry and Civil and Environmental Engineering and by the 1U4U program. Nuclear magnetic resonance spectroscopy was recorded at the David M. Grant NMR Center. Funds for the Center and the helium recovery system were obtained from the University of Utah and from National Institutes of Health (NIH) awards 1C06RR017539-01A1 and 3R01GM063540-17W1. Nuclear magnetic resonance spectroscopy instruments were purchased with support from the University of Utah and from NIH award 1S10OD25241-01. Research reported in this publication used the Biorepository and Molecular Pathology Shared Resource at Huntsman Cancer Institute at the University of Utah and was supported by the National Cancer Institute of the NIH under award P30CA042014. The content is solely the responsibility of the authors and does not necessarily represent the official views of the NIH. Research was partially funded by the NRC Graduate Research Fellowship under award

31310019M0042. No other potential conflict of interest relevant to this article was reported.

## ACKNOWLEDGMENTS

$^{225}$Ac used in this research was supplied by the U.S. Department of Energy Isotope Program, managed by the Office of Isotope R&D and Production. We acknowledge the Cell Imaging Core at the University of Utah for use of the Axio Scan.Z1 slide scanner and thank Dr. Michael John Bridge for assistance in image acquisition.

**KEY POINTS**

**QUESTION:** Does TAT reduce amyloid plaque burden?

**PERTINENT FINDINGS:** In vitro assays showed reduction of amyloid-β when exposed to TAT. Compound **8** was shown to bind selectively while radiolabeled with a high specific activity.

**IMPLICATIONS FOR PATIENT CARE:** TAT should be studied in vivo for its effects on amyloid-β plaques and activation of the immune system as a therapeutic route for AD.

## REFERENCES

1. 2020 Alzheimer's disease facts and figures. *Alzheimers Dement.* 2020;16:391–460.
2. FDA grants accelerated approval for Alzheimer's disease treatment. News release. Food and Drug Administration; January 6, 2023.
3. van Dyck CH, Swanson CJ, Aisen P, et al. Lecanemab in early Alzheimer's disease. *N Engl J Med.* 2023;388:9–21.
4. Cummings JL, Tong G, Ballard C. Treatment combinations for Alzheimer's disease: current and future pharmacotherapy options. *J Alzheimers Dis.* 2019;67:779–794.
5. Forner S, Baglietto-Vargas D, Martini AC, Trujillo-Estrada L, LaFerla FM. Synaptic impairment in Alzheimer's disease: a dysregulated symphony. *Trends Neurosci.* 2017;40:347–357.
6. Jack CR Jr, Bennett DA, Blennow K, et al. NIA-AA research framework: toward a biological definition of Alzheimer's disease. *Alzheimers Dement.* 2018;14:535–562.
7. Meier-Stephenson FS, Meier-Stephenson VC, Carter MD, et al. Alzheimer's disease as an autoimmune disorder of innate immunity endogenously modulated by tryptophan metabolites. *Alzheimers Dement (N Y).* 2022;8:e12283.
8. Kim S, Chung H, Ngoc Mai H, et al. Low-dose ionizing radiation modulates microglia phenotypes in the models of Alzheimer's disease. *Int J Mol Sci.* 2020;21:4532.
9. Ceyzériat K, Millet P, Frisoni GB, Garibotto V, Zilli T. Low-dose radiation therapy: a new treatment strategy for Alzheimer's disease? *J Alzheimers Dis.* 2020;74:411–419.
10. Choi SY, Kwon N, Kim ST, et al. The effect of low dose radiation on Alzheimer's disease-induced TG mice [abstract]. *Int J Radiat Oncol Biol Phys.* 2018;102 (suppl):E210–E211.
11. Wilson GD, Wilson TG, Hanna A, et al. Low dose brain irradiation reduces amyloid-β and tau in 3xTg-AD mice. *J Alzheimers Dis.* 2020;75:15–21.
12. Hwang S, Jeong H, Hong EH, Joo HM, Cho KS, Nam SY. Low-dose ionizing radiation alleviates Aβ42-induced cell death via regulating AKT and p38 pathways in *Drosophila* Alzheimer's disease models. *Biol Open.* 2019;8:bio036657.
13. Cuttler JM, Abdellah E, Goldberg Y, et al. Low doses of ionizing radiation as a treatment for Alzheimer's disease: a pilot study. *J Alzheimers Dis.* 2021;80:1119–1128.
14. Chung M, Rhee HY, Chung WK. Clinical approach of low-dose whole-brain ionizing radiation treatment in Alzheimer's disease dementia patients. *J Alzheimers Dis.* 2021;80:941–947.
15. Rogers CL, Lageman SK, Fontanesi J, et al. Low-dose whole brain radiation therapy for Alzheimer's dementia: results from a pilot trial in human subjects. *Int J Radiat Oncol Biol Phys.* 2023;117:87–95.
16. Okumura H, Itoh SG. Molecular dynamics simulation studies on the aggregation of amyloid-beta peptides and their disaggregation by ultrasonic wave and infrared laser irradiation. *Molecules.* 2022;27:2483.
17. Kalita S, Bergman H, Dubey KD, Shaik S. How can static and oscillating electric fields serve in decomposing Alzheimer's and other senile plaques? *J Am Chem Soc.* 2023;145:3543–3553.
18. Jadvar H. Targeted alpha-therapy in cancer management: synopsis of preclinical and clinical studies. *Cancer Biother Radiopharm.* 2020;35:475–484.
19. Eychenne R, Cherel M, Haddad F, Guerard F, Gestin JF. Overview of the most promising radionuclides for targeted alpha therapy: the "hopeful eight." *Pharmaceutics.* 2021;13:906.
20. Parker C, Lewington V, Shore N, et al. Targeted alpha therapy, an emerging class of cancer agents: a review. *JAMA Oncol.* 2018;4:1765–1772.
21. Birnbaum ER, Fassbender ME, Ferrier MG, John KD, Mastren T. Actinides in medicine. In: Hanuwa TP, Evans WJ, eds. *The Heaviest Metals: Science and Technology of the Actinides and Beyond.* Wiley; 2019:445.
22. Nelson BJB, Andersson JD, Wuest F. Targeted alpha therapy: progress in radionuclide production, radiochemistry and applications. *Pharmaceutics.* 2020;13:1–28.
23. Kratochwil C, Bruchertseifer F, Giesel FL, et al. $^{225}$Ac-PSMA-617 for PSMA-targeted α-radiation therapy of metastatic castration-resistant prostate cancer. *J Nucl Med.* 2016;57:1941–1944.
24. Kunos CA, Mankoff DA, Schultz MK, Graves SA, Pryma DA. Radiopharmaceutical chemistry and drug development—what's changed? *Semin Radiat Oncol.* 2021; 31:3–11.
25. Yang EJ, Kim H, Choi Y, et al. Modulation of neuroinflammation by low-dose radiation therapy in an animal model of Alzheimer's disease. *Int J Radiat Oncol Biol Phys.* 2021;111:658–670.
26. Pulgar VM. Transcytosis to cross the blood brain barrier, new advancements and challenges. *Front Neurosci.* 2019;12:1019.
27. Wang Y, Mathis CA, Huang G-F, et al. Effects of lipophilicity on the affinity and nonspecific binding of iodinated benzothiazole derivatives. *J Mol Neurosci.* 2003;20: 255–260.
28. Cheng Y, Ono M, Kimura H, Ueda M, Saji H. Technetium-99m labeled pyridyl benzofuran derivatives as single photon emission computed tomography imaging probes for beta-amyloid plaques in Alzheimer's brains. *J Med Chem.* 2012;55:2279–2286.
29. Márquez F, Yassa MA. Neuroimaging biomarkers for Alzheimer's disease. *Mol Neurodegener.* 2019;14:21.
30. Kirkeby EK, Chyan MK, Diehl G, et al. Design and synthesis of astatinated benzothiazole compounds for their potential use in targeted alpha therapy (TAT) strategies to treat Alzheimer's disease-associated amyloid plaques. *Appl Radiat Isot.* 2023;191:110555.
31. Kato H, Huang X, Kadonaga Y, et al. Intratumoral administration of astatine-211-labeled gold nanoparticle for alpha therapy. *J Nanobiotechnology.* 2021;19:223.
32. Zalutsky MR, Pruszynski M. Astatine-211: production and availability. *Curr Radiopharm.* 2011;4:177–185.
33. Radchenko V, Morgenstern A, Jalilian AR, et al. Production and supply of α-particle–emitting radionuclides for targeted α-therapy. *J Nucl Med.* 2021;62:1495–1503.
34. Ferrier MG, Radchenko V, Wilbur DS. Radiochemical aspects of alpha emitting radionuclides for medical application. *Radiochim Acta.* 2019;107:1065–1085.
35. Xu H, Wong KJ, Brechbiel MW. A novel bifunctional maleimido CHX-A″ chelator for conjugation to thiol-containing biomolecules. *Bioorg Med Chem Lett.* 2008; 18:2679–2683.
36. De Ferrari GV, Mallender WD, Inestrosa NC, Rosenberry TL. Thioflavin T is a fluorescent probe of the acetylcholinesterase peripheral site that reveals conformational interactions between the peripheral and acylation sites. *J Biol Chem.* 2001; 276:23282–23287.
37. Martins AF, Dias DM, Morfin JF, et al. Interaction of PiB-derivative metal complexes with beta-amyloid peptides: selective recognition of the aggregated forms. *Chemistry.* 2015;21:5413–5422.
38. Tiiman A, Palumaa P, Tõugu V. The missing link in the amyloid cascade of Alzheimer's disease: metal ions. *Neurochem Int.* 2013;62:367–78.
39. LeVine H III. Quantification of beta-sheet amyloid fibril structures with thioflavin T. *Methods Enzymol.* 1999;309:274–284.
40. Fodero-Tavoletti MT, Rowe CC, McLean CA, et al. Characterization of PiB binding to white matter in Alzheimer disease and other dementias. *J Nucl Med.* 2009;50:198–204.
41. Yiannopoulou KG, Papageorgiou SG. Current and future treatments for Alzheimer's disease. *Ther Adv Neurol Disord.* 2013;6:19–33.
42. O'Reilly MA, Waspe AC, Ganguly M, Hynynen K. Focused-ultrasound disruption of the blood-brain barrier using closely-timed short pulses: influence of sonication parameters and injection rate. *Ultrasound Med Biol.* 2011;37:587–594.
43. Ceyzériat K, Zilli T, Fall AB, et al. Treatment by low-dose brain radiation therapy improves memory performances without changes of the amyloid load in the TgF344-AD rat model. *Neurobiol Aging.* 2021;103:117–127.
44. Ceyzériat K, Tournier BB, Millet P, et al. Low-dose radiation therapy reduces amyloid load in young 3xTg-AD mice. *J Alzheimers Dis.* 2022;86:641–653.
45. Ceyzériat K, Zilli T, Millet P, et al. Low-dose brain irradiation normalizes TSPO and CLUSTERIN levels and promotes the non-amyloidogenic pathway in presymptomatic TgF344-AD rats. *J Neuroinflammation.* 2022;19:311.
46. Ceyzériat K, Jaques E, Gloria Y, et al. Low-dose radiation therapy impacts microglial inflammatory response without modulating amyloid load in female TgF344-AD rats. *J Alzheimers Dis.* 2024;98:1001–1016.